EPJ Plus

EPJ.org
your physics journal

Eur. Phys. J. Plus (2019) **134**: 107 DOI 10.1140/epjp/i2019-12447-y

Darcy-Forchheimer flow and heat transfer of water-based Cu nanoparticles in convergent/divergent channel subjected to particle shape effect

K. Ganesh Kumar and Ali J. Chamkha

Società Italiana di Fisica

Springer

Eur. Phys. J. Plus (2019) **134**: 107
DOI 10.1140/epjp/i2019-12447-y

THE EUROPEAN PHYSICAL JOURNAL PLUS

Regular Article

Darcy-Forchheimer flow and heat transfer of water-based Cu nanoparticles in convergent/divergent channel subjected to particle shape effect

K. Ganesh Kumar[1,a] and Ali J. Chamkha[2,3,b]

[1] Department of Mathematics, SJM Institute of Technology, Chitradurga - 577502, Karnataka, India
[2] Mechanical Engineering Department, Prince Sultan Endowment for Energy and Environment, Prince Mohammad Bin Fahd University, Al-Khobar 31952, Saudi Arabia
[3] RAK Research and Innovation Center, American University of Ras Al Khaimah, Ras Al Khaimah, United Arab Emirates

Received: 23 January 2018 / Revised: 13 November 2018
Published online: 18 March 2019

Abstract. The current study provides a comprehensive numerical investigation of flow and heat transfer of water-based Cu nanoparticles over a convergent/divergent channel. In order to control the random motion of nanoparticles, Darcy-Forchheimer, particle shape effect and viscous dissipation are also incorporated for the present mechanism. The resulting system of nonlinear equations is solved numerically by using the RKF-45 method. Expressions for the velocity and temperature profile are derived and plotted under the assumption of a flow parameter. The influence of various parameters on surface drag force and heat transfer rates have been discussed with the help of tables and plots.

Introduction

Flow over a converging and diverging channel is an essential part of any physical model due to its wide range of applications, such as, aerospace, chemical, mechanical, civil, environmental and bio-mechanical engineering, etc. Jeffery and Hamel [1,2] presented pioneer efforts in the area of converging/diverging channels. On the basis of the above work a few studies have investigated the influence of converging/diverging channels. Motsa *et al.* [3] presented on a new analytical method for flow between two inclined walls. Asadullah *et al.* [4] initiated the MHD flow of a Jeffery fluid in converging and diverging channels. Muhammad *et al.* [5] discussed the least square study of heat transfer over a converging/diverging channel. Syed *et al.* [6] studied the MHD flow of a nanofluid in the presence of convergent/divergent channels. Ahmed *et al.* [7] investigated the thermal radiation effects on the flow of a Jeffery fluid in converging and diverging stretchable channels. Babaelahi [8] investigated an analytic approximate solution for a flow of a second-grade viscoelastic fluid in a converging porous channel.

The mechanism of the flow and heat transfer of nanoparticle shapes has been the topic of extensive research due to its widely implementation in the engineering areas including solar collectors electronics, optics, catalysis, materials, smart computers, solar cells, renewable energy. Due to these applications, Xie *et al.* [9] studied the thermal conductivity enhancement of suspensions containing nanosized alumina particles. Timofeeva *et al.* [10] discussed the particle shape effects on thermophysical properties of alumina nanofluids. Lin *et al.* [11] incorporated the effect of radiation with exponential temperature on a Marangoni boundary layer flow. Some important references in the literature concerning nanoparticle shapes can be found in refs. [12–19].

The analysis of heat transfer through a porous medium has increased tremendously in the present world of engineering and industrial applications, such as nuclear waste disposal, crude oil production, grain storage, porous insulation, petroleum reservoirs, ground water pollution, packed bed reactors and resin transfer modeling, etc. Forchheimer [20] considered such factors by using the additional term through square velocity in the Darcian velocity expression. Muskat [21] presented the flow of homogeneous fluids through porous media. Seddeek [22] analyzed the effect of viscous dissipation on a Darcy-Forchheimer mixed convection flow in a porous media. Pal and Mondal [23] initiated the

[a] e-mail: ganikganesh@gmail.com
[b] e-mail: achamkha@yahoo.com

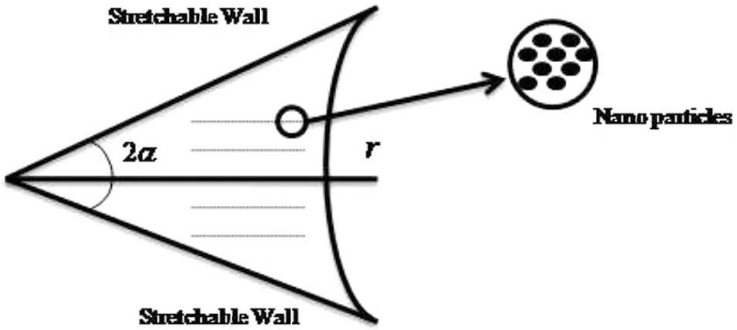

Fig. 1. Schematic diagram of the flow problem.

hydromagnetic convective diffusion of species in a Darcy-Forchheimer porous medium. Recently, various studies of Darcy-Forchheimer can be found in [24–30].

The Darcy-Forchheimer porous medium and particle shape effect on converging and diverging channels have not received due attention so far. This paper will help to fill this void by presenting a detailed analysis of flow and heat transfer of Cu water nanoparticles over a converging and diverging channel in the presence of viscous dissipation. Such flow is taken into account for the Darcy-Forchheimer porous medium and particle shape effects. Numerical values of flow and heat transfer rates are presented in the tables. Moreover, the influence of embedded parameters on velocity and temperature is discussed and illustrated graphically.

Mathematical formulation

It is assumed flow through sink and source at the intersection of two plane walls which make an angle 2α between each other. The geometry of the problem is given in fig. 1. The walls are supposed to be shrinking/ stretching at a rate of S and that velocity at the wall can be stated as $\widehat{u}_r = U_w = \frac{s}{r}$. Moreover, the channel is considered to be saturated by the nanofluid containing the base fluid (water) and copper (Cu) nanoparticles. Between the base fluid and the nanoparticles, a thermal equilibrium is assumed.

We used a polar coordinate system (r, θ) to formulate the mentioned flow problem. The velocity field proceeds to the form $V = [\hat{u}_r, 0, 0]$, where $\hat{u}_r$ is a function both of r and θ Hence, the continuity, momentum and energy equations in polar form due to practical assumptions reduced to the following:

$$\frac{1}{r}\frac{\partial}{\partial r}(r\hat{u}_r) = 0, \tag{1}$$

$$\rho_{nf}\left(\hat{u}_r\frac{\partial \hat{u}_r}{\partial r}\right) = -\frac{\partial p}{\partial r} + \mu_{nf}\left[\frac{\partial^2 \hat{u}_r}{\partial r^2} + \frac{1}{r}\frac{\partial \hat{u}_r}{\partial r} + \frac{1}{r^2}\frac{\partial^2 \hat{u}_r}{\partial \theta^2} - \frac{\hat{u}_r}{r^2}\right] - \frac{\nu_f}{k}\hat{u}_r - F{\hat{u}_r}^2, \tag{2}$$

$$-\frac{1}{\rho_{nf} r}\frac{\partial p}{\partial \theta} + \frac{2}{r^2}\frac{\mu_{nf}}{\rho_{nf}}\frac{\partial \hat{u}_r}{\partial \theta} = 0\,, \tag{3}$$

$$\hat{u}_r\frac{\partial \hat{T}}{\partial r} = \frac{k_{nf}}{(\rho C_p)_{nf}}\left[\frac{\partial^2 \hat{T}}{\partial r^2} + \frac{1}{r}\frac{\partial \hat{T}}{\partial r} + \frac{1}{r^2}\frac{\partial^2 \hat{T}}{\partial \theta^2}\right] + \mu_{nf}\left[4\left(\frac{\partial \hat{u}_r}{\partial r}\right)^2 + \frac{1}{r^2}\left(\frac{\partial \hat{u}_r}{\partial \theta}\right)^2\right]. \tag{4}$$

Boundary conditions for the problem are

$$\begin{aligned} &\hat{u}_r = U, \quad \frac{\partial \hat{u}_r}{\partial \theta} = 0, \quad \frac{\partial \hat{T}}{\partial \theta} = 0 \quad \text{at } \theta = 0, \\ &\hat{u}_r = U_w, \quad \hat{T} = \frac{\hat{T}_w}{r^2} \quad \text{at } \theta = \alpha. \end{aligned} \tag{5}$$

In the above equations, U is the centerline velocity of the channel, $\hat{T}_w$, U_w the temperature and velocity at the channel wall respectively, k the permeability of porous medium, $F = \frac{c_b}{rk^{\frac{1}{2}}}$ the non-uniform inertia coefficient of porous medium, c_b the drag coefficient. Further, ρ_{nf}, μ_{nf}, $(\rho C_p)_{nf}$ and k_{nf} denote the density, dynamic viscosity, heat capacity and

thermal conductivity of the fluid, respectively,

$$\rho_{nf} = (1-\phi)\rho_f + \phi\rho_s, \qquad \mu_{nf} = \frac{\mu_f}{(1-\phi)^{2.5}},$$
$$\frac{k_{nf}}{k_f} = \frac{[k_s + (m-1)k_f] - (m-1)\phi(k_f - k_s)}{[k_s + (m-1)k_f] + \phi(k_f - k_s)}, \qquad (\rho c_p)_{nf} = (1-\phi)(\rho c_p)_f + \phi(\rho c_p)_s, \tag{6}$$

where ϕ is the solid volume fraction of the nanofluid, ρ_f is the density of the base fluid, ρ_s is the density of nanoparticles, μ_f is the dynamic viscosity of the base fluid, $(\rho c_p)_f$ is the heat capacity of the base fluid, $(\rho c_p)_s$ is the heat capacity of nanoparticles, k_f is the thermal conductivity of the base fluid and k_s is the thermal conductivity of nanoparticles and m-particle shape.

Equation (1) provides a pure depiction of the radial velocity form as follows:

$$F(\theta) = r\hat{u}_r(r,\theta). \tag{7}$$

The following non-dimensional variables are used:

$$f(\eta) = \frac{F(\theta)}{U}, \qquad \eta = \frac{\theta}{\alpha}, \qquad \Theta = r^2\frac{T}{T_w}. \tag{8}$$

The implementation of similarity transformation given in eq. (8) besides the elimination of the pressure terms from eqs. (2) and (3) provides coupled equations for the following temperature and velocity profiles:

$$f''' + 2\alpha Re(1-\phi)^{2.5}\left[(1-\phi) + \phi\frac{\rho_s}{\rho_f}\right]ff' + \left(4 - Kp(1-\phi)^{2.5}\left[(1-\phi) + \phi\frac{\rho_s}{\rho_f}\right]\right)\alpha^2 f'$$
$$+ 2\alpha^2 Fr(1-\phi)^{2.5}\left[(1-\phi) + \phi\frac{\rho_s}{\rho_f}\right]f'^2 = 0, \tag{9}$$
$$\frac{k_{nf}}{k_f}\left(\Theta'' + 4\alpha^2\Theta\right) + 2Pr\left[(1-\phi) + \phi\frac{\rho_s}{\rho_f}\right]\alpha^2\Theta f + \frac{PrEc}{Re(1-\phi)^{2.5}}\left[(1-\phi) + \phi\frac{\rho_s}{\rho_f}\right](4\alpha^2 f^2 + f'^2) = 0. \tag{10}$$

The reduced appropriate boundary conditions due to eq. (10) are as follows:

$$f(\eta) = 1, \quad f'(\eta) = \Theta'(\eta) = 0, \quad \text{at } \eta = 0,$$
$$f(\eta) = S, \quad \Theta(\eta) = 1, \quad \text{as } \eta = 1. \tag{11}$$

In eq. (14), S is indicating the shrinking/stretching parameter that is for stretchable walls is $S > 0$, and $S < 0$, is for shrinking walls, $Re = \frac{U_c\alpha}{\nu_f}$ is the Reynolds number, for divergent channel $\alpha > 0$, and convergent channel $\alpha < 0$, $Kp = \frac{\nu_f}{kU_c}$ is the porosity parameter, $Fr = \frac{c_b}{k^{\frac{1}{2}}}$ is the inertia coefficient, $Ec = \frac{U_c^2\alpha}{k_{nf}}$ is the Eckert number, $Pr = \frac{(\rho C_p)_f}{k_{nf}}$ is the Prandtl number.

Physical quantities of interest, the skin friction coefficient and Nusselt number are defined as follows:

$$C_f = \frac{\mu_{nf}(\tau_{r\theta})_{nf}}{\rho_{nf}{U_c}^2} \quad \text{and} \quad Nu = -\frac{k_f(q_w)_{n=1}}{kT_w}.$$

In terms of eqs. (6)–(8) as follows:

$$ReC_f = \frac{1}{(1-\phi)^{2.5}[(1-\phi) + \phi\frac{\rho_s}{\rho_f}]}f'(1) \quad \text{and} \quad \alpha Nu = -\frac{[k_s + (m-1)k_f] - (m-1)\phi(k_f - k_s)}{[k_s + (m-1)k_f] + \phi(k_f - k_s)}\Theta'(1).$$

Solution procedure

The reduced flow governing coupled ordinary differential equations (9)-(10) along with the boundary limitations (11) are resolved numerically using the Runge-Kutta based procedure along with the shooting method. Initially, the set of coupled nonlinear ordinary differential equations (9)–(11) are converted to a system of first-order differential equations using the following procedure:

Table 1. Thermo-physical properties of Cu-water nanoparticles.

	ρ (kg/m^3)	C_p (j/kgk)	k (W/mk)
H_2O	997.1	4179	0.613
Cu	8.933	385	400

Table 2. The value of parameters for thermal conductive and viscosity models.

Particle Shapes	Sphere	Column	Lamina
m	3	6.3698	16.1576

Let $f = y_1$, $f' = y_2$, $f'' = y_3$, $\Theta = y_4$, $\Theta' = y_5$, then

$$y_3' = -2\alpha Re(1-\phi)^{2.5}\left[(1-\phi)+\phi\frac{\rho_s}{\rho_f}\right]y_1y_2 - \left(4 - Kp(1-\phi)^{2.5}\left[(1-\phi)+\phi\frac{\rho_s}{\rho_f}\right]\right)\alpha^2 y_2$$

$$- 2\alpha^2 Fr(1-\phi)^{2.5}\left[(1-\phi)+\phi\frac{\rho_s}{\rho_f}\right]{y_2}^2 = 0, \tag{12}$$

$$y_5' = \frac{1}{\frac{k_{nf}}{k_f}}\left[2Pr\left[\phi\frac{\rho_s}{\rho_f}-(1-\phi)\right]\alpha^2 y_4y_1 + \frac{PrEc}{Re(1-\phi)^{2.5}}\left[(1-\phi)+\phi\frac{\rho_s}{\rho_f}\right](4\alpha^2{y_1}^2 - {y_2}^2)\right] - 4\alpha^2 y_4, \tag{13}$$

and the corresponding boundary conditions will become:

$$y_1 = 1, \quad y_2 = y_5 = 0, \quad \text{at } \eta = 0,$$
$$y_1 = S, \quad y_4 = 1, \quad \text{as } \eta = 1. \tag{14}$$

With the aid of the shooting technique, omitted initial conditions are predicted. This technique is an iterative algorithm to determine the appropriate initial conditions for a relevant initial value problem that provides the solution to the original boundary value problem. We have considered infinity condition at a large but finite value of η.

After fixing the finite value for η_∞, integration is carried out with the help of the RKF-45 method. This method has a procedure to determine an accurate solution if the proper step size h is being used. At each step, two different approximations for the solution are made and compared. If the two answers are in close agreement, the approximation is accepted otherwise the step size is reduced until getting the required accuracy. For the present problem, we took step size $\Delta\eta = 0.001$, $\eta_\infty = 1$ and accuracy to the fifth decimal place.

Result and discussion

Similarity equalities (12)-(13) with the border ailment (14) are highly non-linear coupled ODE's. This complicated system is very difficult to solve with the usual analytical method. So we apply the RKF-45 numerical method based on the shooting technique. Numerical results for flow velocity and temperature profiles for a choice of values of physical parameters are illustrated with plotted graphs. Numerical values of friction factor coefficients and local Nusselt are shown in tabular forms.

Table 1 displays the properties of physical and thermal interest linked to the base fluid and nanoparticles. These properties are used to explore the changes emerging in velocity and temperature profiles subject to the variations in different parameters. Table 2 shows the different shape particles. Table 3 presents the values of the local skin friction coefficient as well as the local Nusselt number for various values of existing parameters in the flow problem. It is recognized that the local skin friction coefficient decreases for F_r, Kp and S but it increases for the remaining parameters, while the number decreases for F_r, Re, ϕ and increases for the persisting parameters. Table 4 represents the skin friction coefficient and Nusselt number for various values of parameters for the converging channel and diverging channel in which $\alpha > 0$ is considered for the converging channel and $\alpha < 0$ for the diverging channel. Here, one can infer that this table shows the same behavior as table 3. Further, the rate of heat transfer is increased in the diverging channel when compared to the converging channel and the surface drag force is lesser in the diverging channel when compared to the converging channel. Table 5 is drawn to see the behavior of different shaped particles on the Nusselt number for various values of existing parameters in the flow problem. From this table we observe that the rate of heat transfer is enhancing more in sphere shaped particles when compare to column and lamina shaped particles.

Table 3. Numerical values of the skin friction coefficient and Nusselt number for different physical parameters.

α	Ec	Fr	Kp	Pr	Re	S	ϕ	$-Nu$	$-ReC_f$
1								1.19094	0.08805
2								3.93590	0.21215
3								7.84646	0.42806
	0.2							2.38188	0.42806
	0.4							4.76377	0.43206
	0.6							7.14566	0.44159
		0.5						1.19526	0.42347
		1						1.18946	0.41797
		15						1.17959	0.39322
			0.5					1.18775	0.45156
			1					1.19307	0.43478
			1.5					1.19837	0.42806
				5				0.99245	0.42806
				6				1.19094	0.42806
				7				1.38943	0.42806
					5			1.19094	0.43034
					6			1.18221	0.43430
					7			1.17586	0.61091
						0.2		1.08627	0.49789
						0.4		1.13542	0.42806
						0.6		1.26678	0.35161
							0.1	1.19094	0.42692
							0.2	0.90749	0.42806
							0.3	0.69735	0.44554

Table 4. Comparison of numerical values of the skin friction coefficient and Nusselt number for both convergent and divergent channel with different physical parameters.

Ec	Fr	Kp	Pr	Re	S	ϕ	$-Nu$		$-ReC_f$	
							$\alpha > 0$	$\alpha < 0$	$\alpha > 0$	$\alpha < 0$
0.2							2.38188	1.69886	0.42806	1.20569
0.4							4.76377	3.39773	0.43606	1.20569
0.6							7.14566	5.09660	0.44159	1.20569
	0.5						1.19526	0.85303	0.42347	1.24349
	1						1.18946	0.84819	0.39322	1.19274
	15						1.17959	0.83977	0.41797	1.10578
		0.5					1.18775	0.84775	0.43478	1.19174
		1					1.19307	0.85054	0.45156	1.21494
		1.5					1.19837	0.85331	0.42806	1.23787
			5				0.99245	0.70786	0.42806	1.20569
			6				1.19094	0.84943	0.42806	1.20569
			7				1.38943	0.99100	0.42806	1.20569
				5			1.19094	0.84943	0.43034	1.20569
				6			1.18221	0.87615	0.43431	1.38924
				7			1.17586	0.90440	0.61091	1.59476
					0.2		1.08627	0.87545	0.49789	1.76643
					0.4		1.13542	0.84864	0.35161	1.40504
					0.6		1.266788	0.85976	0.42806	0.99314
						0.1	1.19094	1.85287	0.42692	2.78913
						0.2	0.90749	1.23666	0.44554	1.79911
						0.3	0.69735	0.84943	0.42806	1.20569

Table 5. Numerical values of the Nusselt number for different shape particles with various physical parameters.

α	Ec	Fr	Kp	Pr	Re	S	ϕ	$-Nu$		
								Sphere	Column	Lamina
1								1.19094	0.93280	0.57729
2								3.93590	3.08278	1.90786
3								7.84646	6.14571	3.80345
	0.2							2.38188	1.86560	1.15458
	0.4							4.76377	3.73121	2.30916
	0.6							7.14566	5.59681	3.46375
		0.5						1.19526	0.93618	0.57938
		1						1.18946	0.93164	0.57657
		15						1.17959	0.92391	0.57179
			0.5					1.18775	0.93030	0.57574
			1					1.19307	0.93446	0.57832
			1.5					1.19837	0.93862	0.58089
				5				0.99245	0.77733	0.48107
				6				1.19094	0.93280	0.57729
				7				1.38943	1.08827	0.67350
					5			1.19094	0.93280	0.57729
					6			1.18221	0.92596	0.57305
					7			1.17586	0.92098	0.56998
						0.2		1.08627	0.85081	0.52655
						0.4		1.13542	0.88931	0.55037
						0.6		1.26678	0.99220	0.61405
							0.1	1.19094	0.93280	0.57729
							0.2	0.90749	0.61565	0.32213
							0.3	0.69735	0.43010	0.20657

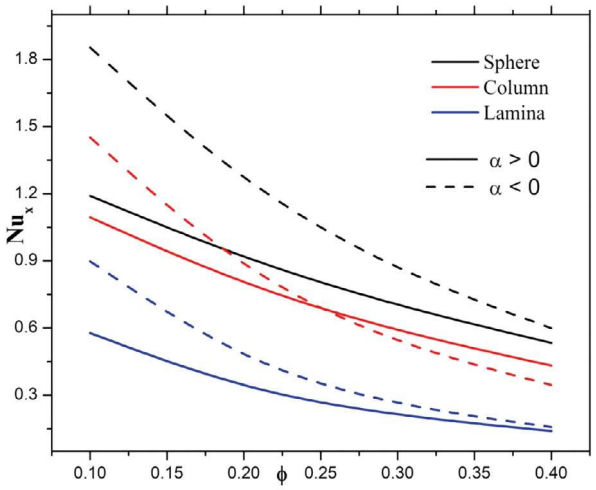

Fig. 2. Effect of ϕ on the Nusselt number.

Figures 2 and 3 are plotted to see the behavior of the nanoparticle volume fraction and stretching ratio parameter on the Nusselt number for different shaped particles. From fig. 2 one can infer that, the Nusselt number is a decreasing function of nanoparticle volume fraction for both converging and diverging channel. Further from these figure we noticed that rate of heat transfer is maximum in converging channel when compeered to diverging channel. Also we observed that, sphere shape particles transfers larger amount of heat when compare to remaining two shape of particles. From fig. 3, for higher values of stretching ratio parameter, Nusselt number as enhancing in diverging channel and decay in converging channel.

Figures 4 and 5 are displayed to depict the impact of opening angle parameter on velocity and temperature. From fig. 4 one can infer that the higher values of the opening angle parameter decay the velocity profile and its corresponding boundary layer thickness. At the center of the channels behavior of the velocity field is dominant. Figure 5 demonstrates the effect of the opening angle on temperature distribution. Here, an enhancement in temperature and its correspondences boundary layer is noticed for enhancing values of the opening angle parameter.

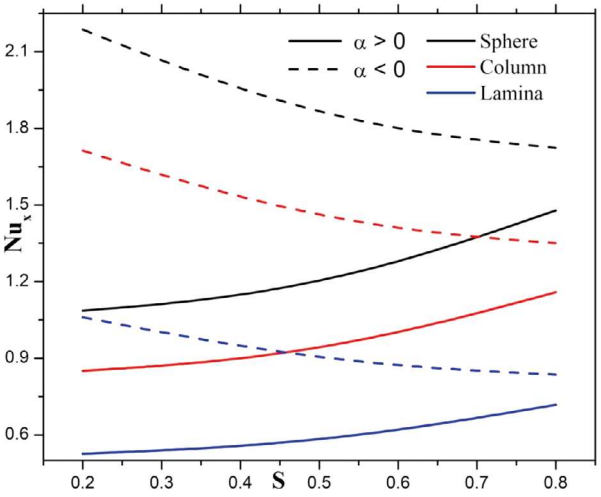

Fig. 3. Effect of S on the Nusselt number.

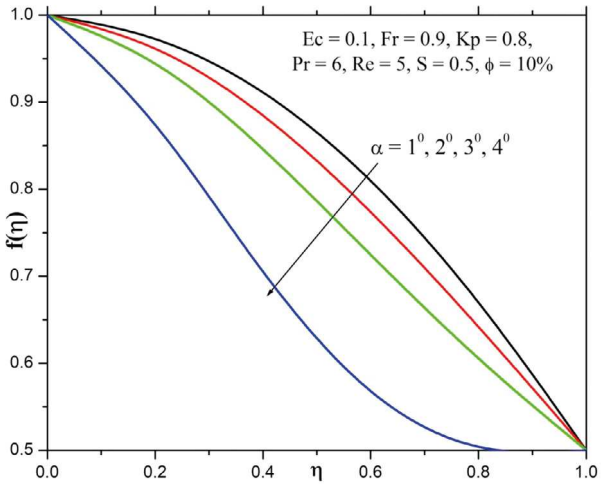

Fig. 4. Effect of α on $f(\eta)$.

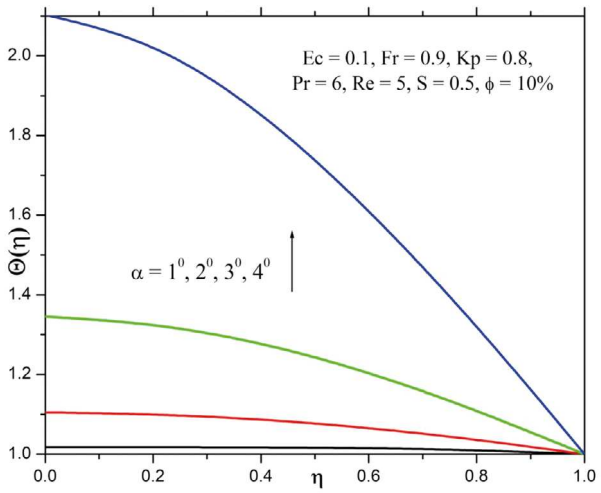

Fig. 5. Effect of α on $\Theta(\eta)$.

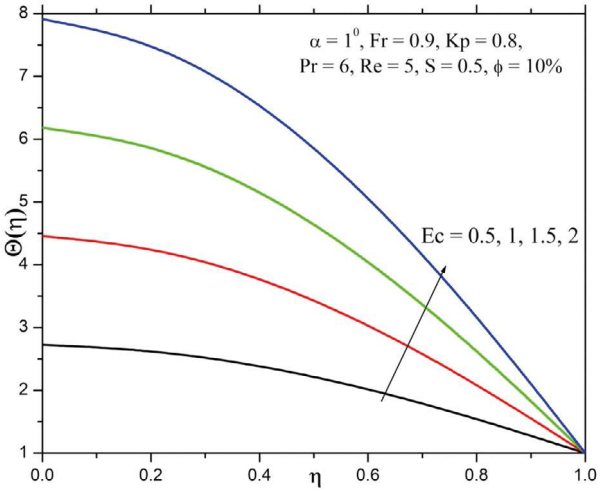

Fig. 6. Effect of Ec on $\Theta(\eta)$.

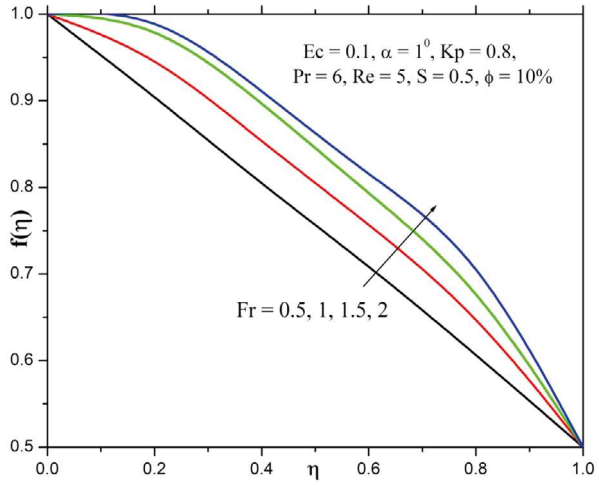

Fig. 7. Effect of Fr on $f(\eta)$.

Figure 6 shows the behavior of the Eckert number on the temperature profile. Both thermal field and corresponding layer thickness are enhanced for higher values of the Eckert number. This is because increasing the value of the Eckert number enhances the kinetic energy and this leads to an increase in the temperature and thermal boundary layer thickness.

Figure 7 depicts the change in the velocity field for the varying inertia coefficient parameter. From the figure we observe that velocity along with the momentum layer thickness enhance as the inertia coefficient parameter rises gradually. Figure 8 captures the influence of the porosity parameter on the velocity field. Here the velocity field is a decreasing function of the higher estimation of the porosity parameter. Physically the presence of a porous media is to increase the resistance to fluid flow which causes a reduction in the velocity profile and a lesser thickness of momentum layer.

The behavior of the Prandtl number on the temperature profile is pictured in fig. 9. Thisfigure shows that the larger estimations of the Prandtl number cause an enhancement in the temperature profile and also increases the thermal boundary layer thickness. It is due to the fact that higher Pr corresponds to lower thermal diffusivity which results in enhancing the temperature field. Figures 10 and 11 show the behavior of the stretching parameter on both velocity and temperature field. From these figure we observe that both velocity and temperature field and their corresponding boundary layer thickness increases by increasing values of the stretching parameter.

Figures 12 and 13 are plotted to see the behavior of the nanoparticle volume fraction on both velocity and temperature field. From fig. 12 we observe that the velocity field and its corresponding boundary layer thickness are enhancing functions of the nanoparticle volume fraction. Figure 13 shows that the decreasing behavior of the temperature field and layer thickness is observed due to nanoparticle volume fraction. Figures 14 and 15 are displayed to depict the impact of the Reynolds number on both velocity and temperature field. From these figures we notice the reduction in velocity and temperature and its corresponding boundary layer thickness for a larger estimation of the Reynolds number.

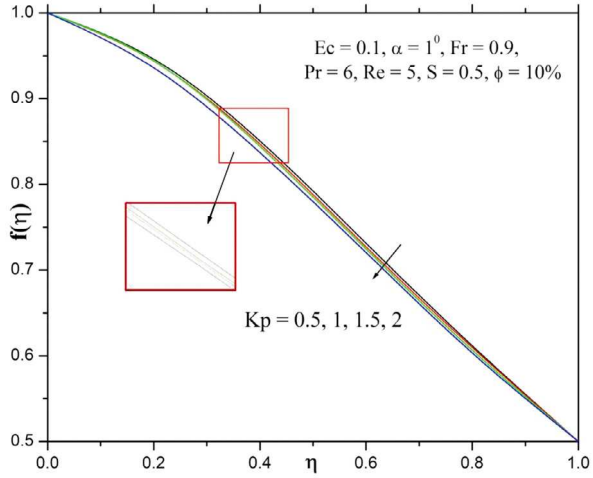

Fig. 8. Effect of Kp on $f(\eta)$.

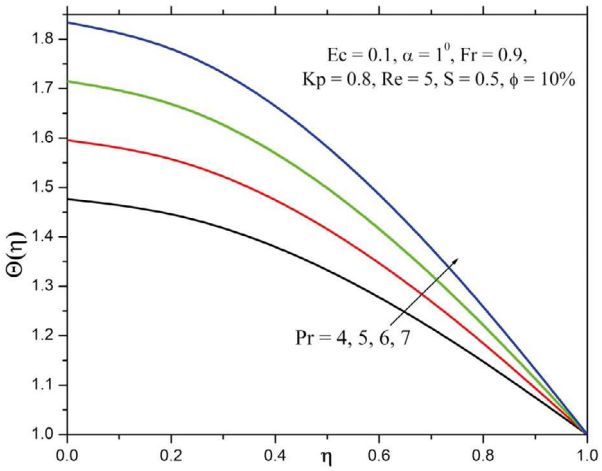

Fig. 9. Effect of Pr on $\Theta(\eta)$.

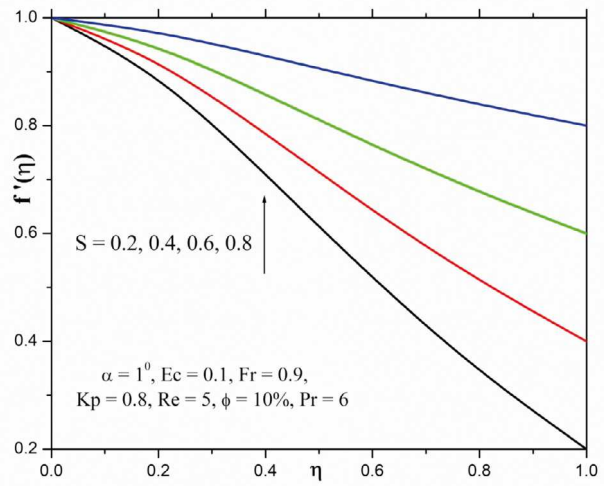

Fig. 10. Effect of S on $f(\eta)$.

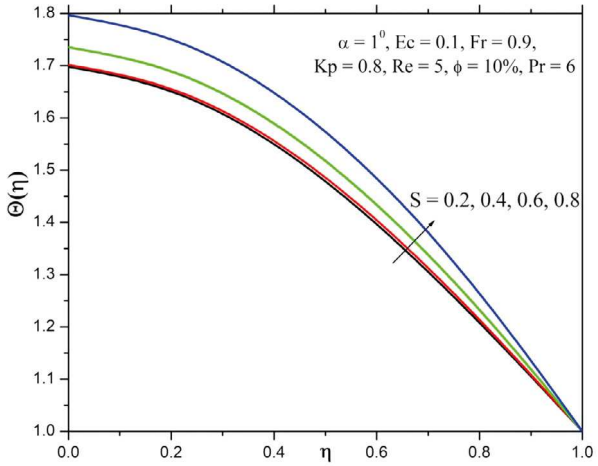

Fig. 11. Effect of S on $\Theta(\eta)$.

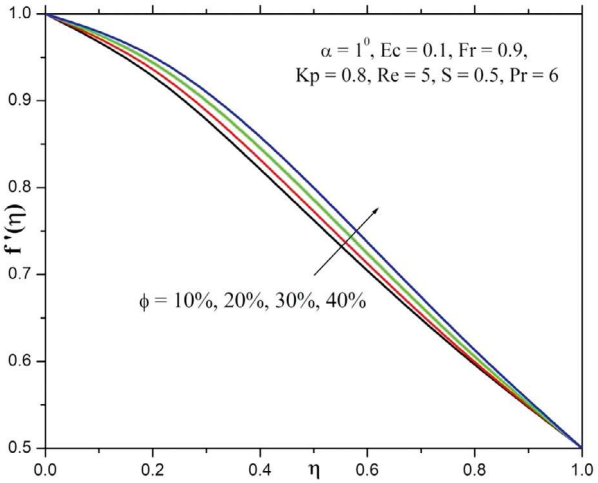

Fig. 12. Effect of ϕ on $f(\eta)$.

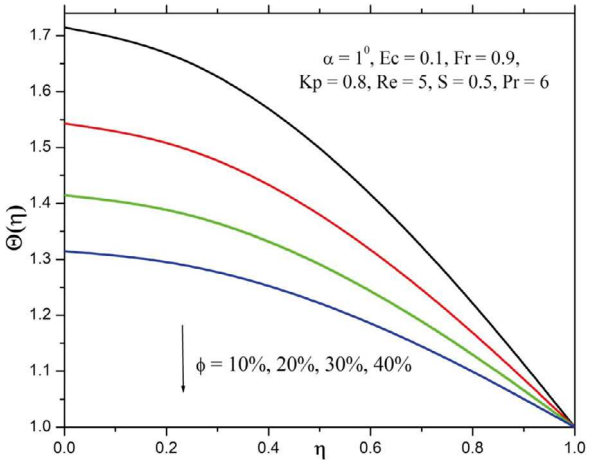

Fig. 13. Effect of ϕ on $\Theta(\eta)$.

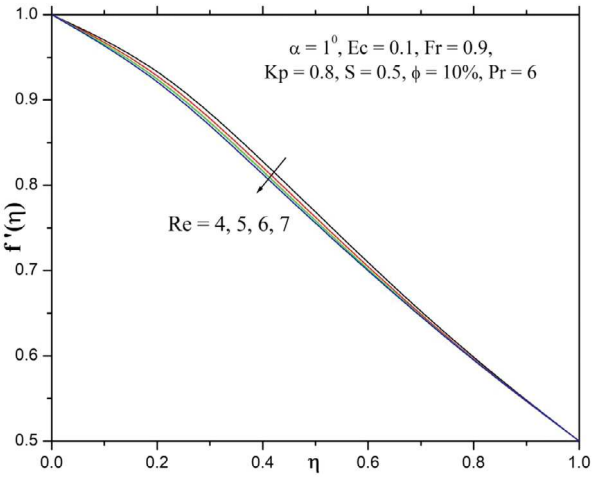

Fig. 14. Effect of Re on $f(\eta)$.

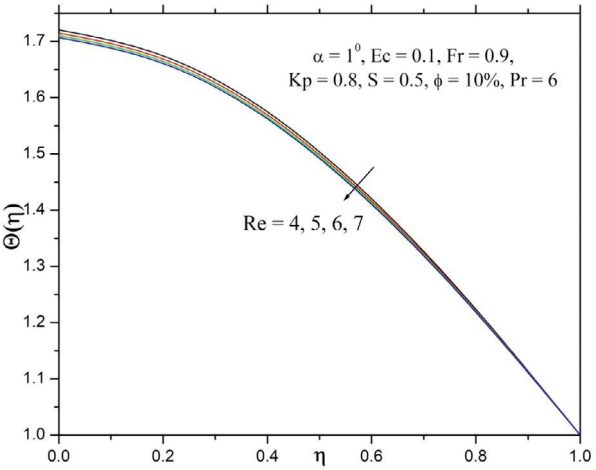

Fig. 15. Effect of Re on $\Theta(\eta)$.

Conclusions

The present study has been carried out to provide a numerical solution for the Darcy-Forchheimer flow and heat transfer of water-based Cu nanoparticles in convergent/divergent channels in the presence of particle shape effect and viscous dissipation. The present flow problem is studied in two cases for the converging and diverging channel condition. The main observations of the present problem are listed below:

- A larger enhancement in temperature is obtained for the sphere shaped particles as compared to column and lamina shaped particles.
- The velocity profile decreases for the increasing values of the porosity parameter, whereas it exhibits the opposite behaviour for the F_r parameter.
- The thermal boundary layer is thicker for the effect of the Eckert number.
- The temperature profile enhances with enlarging values of the Prandtl number.
- An opening angle parameter enhances the rate of transfer and decays the surface drag coefficient.
- The momentum and thermal boundary layer thickness is an enhancing function of the suction parameter.
- Larger values of the Reynolds number scale back the velocity and temperature distribution.

References

1. G.B. Jeffery, London, Edinb. Dublin Philos. Mag. J. Sci. **29**, 455 (1915).
2. G. Hamel, Jahresber. Dtsch. Math. Ver. **25**, 34 (1917).
3. S.S. Motsa, P. Sibanda, G.T. Marewo, Numer. Algorithms **61**, 499 (2012).
4. U. Asadullah, R. Khan, Manzoor, N. Ahmed, S.T. Mohyud-Din, Int. J. Mod. Math. Sci. **6**, 92 (2013).
5. M. Usman, Rizwan Ul Haq, M. Hamid, W. Wang, J. Mol. Liq. **249**, 856 (2018).
6. T.M.D. Syed, U. Khan, N. Ahmed, B.B. Mohsin, Neural Comput. Appl. **28**, 4079 (2017).
7. N. Ahmed, A. Abbasi, U. Khan, S.T. Mohyud-Din, Neural Comput. Appl. **30**, 2371 (2018).
8. M. Babaelahi, J. Appl. Mech. Tech. Phys. **59**, 72 (2018).
9. H.Q. Xie, J.C. Wang, T.G. Xi, Y. Liu, F. Ai, Q.R. Wu, J. Appl. Phys. **91**, 4568 (2012).
10. E.V. Timofeeva, J.L. Routbort, Dileep Singh, J. Appl. Phys. **106**, 014304 (2009).
11. Yanhai Lin, Botong Li, Liancun Zheng, Goong Chen, Powder Technol. **301**, 379 (2016).
12. R. Ellahi, M. Hassan, A. Zeeshan, Ambreen A. Khan, Appl. Nanosci. **6**, 641 (2016).
13. R. Ellahi A. Zeeshan, M. Hassan, Int. J. Numer. Methods Heat Fluid Flow **26**, 2160 (2016).
14. M. Sheikholeslami, M.M. Bhatti, Int. J. Heat Mass Transfer **111**, 1039 (2017).
15. N.S. Akbar, D. Tripathi, O.A. Beg, Adv. Powder Technol. **28**, 453 (2017).
16. E.H. Ooi, V. Popov, Int. J. Therm. Sci. **65**, 178 (2013).
17. Amira Trodi, M.E. Hocine Benhamza, Chem. Eng. Commun. **204**, 158 (2017).
18. Z. Zeeshan, M. Hassan, R. Ellahi, M. Nawaz, Proc. Inst. Mech. Eng., Part E **231**, 871 (2017).
19. U. Khan, Naveed Ahmed, S.T. Mohyud-Din, Neural Comput. Appl. **29**, 695 (2018).
20. P. Forchheimer, Z. Ver. Dtsch. Ing. **45**, 1782 (1901).
21. M. Muskat, *The Flow of Homogeneous Fluids through Porous Media* (Edwards, 1946).
22. M.A. Seddeek, J. Colloids Interface Sci. **293**, 137 (2006).
23. D. Pal, H. Mondal, Int. Commun. Heat Mass Transf. **39**, 913 (2012).
24. T. Hayat, T. Muhammad, S. Al-Mezal, S.J. Liao, Int. J. Numer. Methods Heat Fluid Flow **26**, 2355 (2016).
25. S.A. Shehzad, F.M. Abbasi, T. Hayat, A. Alsaedi, J. Mol. Liq. **224**, 274 (2016).
26. M.A. Meraj, S.A. Shehzad, T. Hayat, F.M. Abbasi, A. Alsaedi, Appl. Math. Mech. **38**, 557 (2017).
27. T. Muhammad, A. Alsaedi, S.A. Shehzad, T. Hayat, Chin. J. Phys. **55**, 963 (2017).
28. T. Hayat, F. Haider, T. Muhammad, A. Alsaedi, PLoS ONE **12**, e0179576 (2017).
29. N. Bano, O.D. Makinde, B.B. Singh, S.R. Sayyed, Diffus. Found. **16**, 140 (2018).
30. M. Sheikholeslami, S.A. Shehzad, Z. Li, A. Shafee, Int. J. Heat Mass Transfer **127**, 614 (2018).